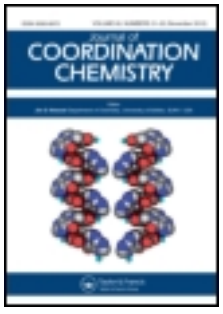

Journal of Coordination Chemistry
Publication details, including instructions for authors and subscription information:
http://www.tandfonline.com/loi/gcoo20

A new imidazophenanthroline derivative and its Hg(II) complex: structures, photophysical properties, and DFT calculations

Zheng Zheng [a] , Zhi-Peng Yu [a] , Hong-Ping Zhou [a] , Jia-Xiang Yang [a] , Yan Feng [a] , Lin Kong [a] , Jie-Ying Wu [a] & Yu-Peng Tian [a b c]

[a] Department of Chemistry , Anhui University and Key Laboratory of Functional Inorganic Materials Chemistry of Anhui Province , 230039 Hefei , PR China

[b] State Key Laboratory of Crystal Materials , Shandong University , 250100 Jinan , PR China

[c] State Key Laboratory of Coordination Chemistry , Nanjing University , 210093 Nanjing , PR China

Accepted author version posted online: 13 Sep 2012.Published online: 27 Sep 2012.

To cite this article: Zheng Zheng , Zhi-Peng Yu , Hong-Ping Zhou , Jia-Xiang Yang , Yan Feng , Lin Kong , Jie-Ying Wu & Yu-Peng Tian (2012) A new imidazophenanthroline derivative and its Hg(II) complex: structures, photophysical properties, and DFT calculations, Journal of Coordination Chemistry, 65:22, 3972-3982, DOI: 10.1080/00958972.2012.729822

To link to this article: http://dx.doi.org/10.1080/00958972.2012.729822

Journal of Coordination Chemistry
Vol. 65, No. 22, 20 November 2012, 3972–3982

A new imidazophenanthroline derivative and its Hg(II) complex: structures, photophysical properties, and DFT calculations

ZHENG ZHENG†, ZHI-PENG YU†, HONG-PING ZHOU*†, JIA-XIANG YANG†, YAN FENG†, LIN KONG†, JIE-YING WU† and YU-PENG TIAN†‡§

†Department of Chemistry, Anhui University and Key Laboratory of Functional Inorganic Materials Chemistry of Anhui Province, 230039 Hefei, PR China
‡State Key Laboratory of Crystal Materials, Shandong University, 250100 Jinan, PR China
§State Key Laboratory of Coordination Chemistry, Nanjing University, 210093 Nanjing, PR China

(*Received 7 May 2012; in final form 14 August 2012*)

A new ligand (**L**) and its mercury(II) complex have been synthesized under mild conditions. X-ray single-crystal structural analyses reveal 1-D, 2-D, and 3-D supermolecular structure of **L** and $HgLI_2$. Solvent molecules and various weak interactions, including hydrogen bonds (N–H···N, O–H···O, and O–H···N) and π–π interactions play significant roles in the final supermolecular structures. Detailed investigation on ^{1}H NMR spectra of **L** and $HgLI_2$ are presented. Their photophysical properties were investigated both experimentally and theoretically.

Keywords: Mercury(II) complex; Crystal structure; ^{1}H NMR spectra; Optical properties; Theoretically

1. Introduction

Recently, organic–inorganic hybrid materials have been of interest for their use in catalysis and molecular separations and due to their fascinating structures [1–7]. Properties are derived from the natural structure and can be subtly moderated by slight structure changes [8]. Self-assembly of molecular building blocks through molecular recognition has led to a number of functional organic and hybrid inorganic–organic materials [9, 10].

Organic bridging ligands play an important role in syntheses directed toward valuating their influence on the formation of different networks. 1,10-Phenanthroline can provide π–π stacking interactions in either intra- or inter-molecular mode, contributing to the stability and formation of extended supramolecular structures [11]. The literature on imidazoles as possible donors to form coordination polymers has expanded rapidly [12–14]. Transition-metal complexes have applications in catalysis,

*Corresponding author. Email: zhpzhp@263.net

ISSN 0095-8972 print/ISSN 1029-0389 online
http://dx.doi.org/10.1080/00958972.2012.729822

adsorption, electric conducting materials, magnetic, optical materials, etc. [15–19]. In contrast to the well-documented Ru-phen complexes, only a few Hg–phen complexes have been reported [20–25]. Therefore, investigation of structures and properties of Hg-phen complexes may provide useful information. The aromatic ring may present a π–π stacking to assemble into a supramolecular structure. Noncovalent interactions (hydrogen bonds and π–π stacking interactions) are useful for supramolecular networks from molecular building blocks.

Here we report the crystal structures of new ligand **(L)** and $HgLI_2$. **L** was prepared according to the literature method with some modification [26], incorporating one imidazole at the terminal (scheme 1). Investigation on the ^1H NMR spectra of **L** and $HgLI_2$ are presented in this article. Theoretical and experimental studies of the photophysical properties of **L** and $HgLI_2$ are also discussed.

2. Experimental

2.1. *Physical measurements*

IR spectra were recorded with a Nicolet FT-IR NEXUS 870 spectrometer (KBr discs) from 4000 to 400 cm^{-1}. ^1H and ^{13}C NMR spectra were recorded on a 400 or 500 MHz NMR instrument using $(CD_3)_2SO$ as a solvent. Chemical shifts are reported in parts per million (ppm) relative to internal TMS (0 ppm) and coupling constants in Hz. Mass spectra were obtained on a Bruker Autoflex III Smartbeam mass spectrometer.

2.2. *Crystal structures determination and refinement*

X-ray diffraction measurements were performed on a Bruker SMART CCD area detector using graphite monochromated Mo-Kα radiation ($\lambda = 0.71069$ Å) at 298 (2) K. Intensity data were collected in the variable ω-scan mode. Structures were solved by direct methods and difference Fourier syntheses. Non-hydrogen atoms were refined anisotropically and hydrogen atoms were introduced geometrically. Calculations were performed with SHELXTL-97.

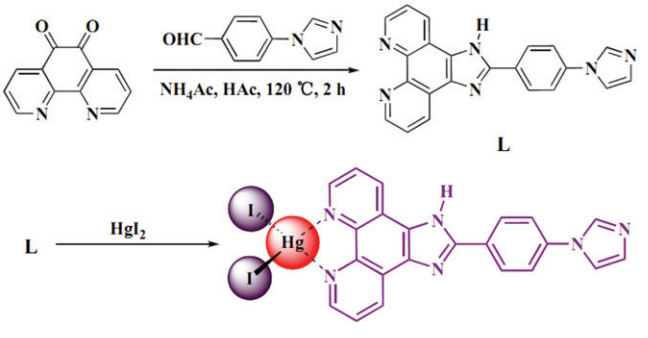

Scheme 1. Synthetic routes to **L** and $HgLI_2$.

2.3. *Computational details*

Calculations were conducted based on the Gauss03 program and the molecular geometry optimization used for the calculation is obtained from single crystal X-ray diffraction crystallographic data. Calculations of **L** based on the density functional theory (DFT) [27] were performed at the rb3lyp/6-311+G(d) level and calculations of $HgLI_2$ were carried out with rb3lyp/6-311+G(d) for C H N atoms and the Lanl2dz basis set for Hg I without any symmetry restraints, which were downloaded from the EMSL basis set library. For calculating absorption spectra, the 25 lowest spin-allowed singlet–singlet transitions, up to 5 eV, were taken into account.

2.4. *Syntheses*

2.4.1. Synthesis of L. A mixture of 4-(1H-imidazol-1-yl)benzaldehyde (0.258 g, 1.5 mmol), 1,10-phenanthroline-5,6-dione (0.315 g, 1.5 mmol), ammonium acetate (2.31 g, 30 mmol), and glacial acetic acid (30 mL) was refluxed for 2 h, then cooled to room temperature and diluted with water (*ca* 60 mL). Dropwise addition of concentrated aqueous ammonia gave a yellow precipitate, which was collected and washed with water. The crude product was purified by recrystallization from a mixture of ethanol and water to get light yellow crystals (0.49 g, yield 90%). Yellow crystalline solid was obtained by slow evaporation at room temperature for one week. m.p.: > 300°C. FT-IR (KBr, cm^{-1}): 3382, 3110, 1611, 1562, 1526, 1494, 1452, 1057, 741, 695. ^{1}H NMR (400 MHz, $(CD_3)_2SO$): δ 13.87 (s, 1H), 9.05 (q, $J = 2.8$ Hz, 2H), 8.94 (d, $J = 8.0$ Hz, 2H), 8.43 (d, $J = 5.2$ Hz, 2H), 8.40 (s, 1H), 7.94 (d, $J = 8.4$ Hz, 2H), 7.91 (s, 1H), 7.85 (q, $J = 8.0$ Hz, 2H), 7.19 (s, 1H). ^{13}C NMR (125 MHz, $(CD_3)_2SO$): δ (ppm) = 150.2, 148.5, 144.3, 138.1, 136.4, 136.1, 130.8, 130.2, 128.8, 128.2, 124.3, 124.1, 123.8, 121.1, 119.8, 118.4. MS, m/z (%): 363.25 (100).

2.4.2. Synthesis of $HgLI_2$. **L** (0.018 g, 0.05 mmol) was added to 5 mL of methanol and 0.027 g (0.06 mmol) of HgI_2 was added slowly with stirring over 5 min, forming a yellow solid immediately. The solution was heated to 60°C for 2 h with stirring. The solid was collected by filtration and washed with methanol, yield was 0.037 g (90%). Yellow crystals were collected after slow evaporation of saturated solution of the crude complex in DMF. m.p.: > 300°C. Anal. Calcd for $C_{22}H_{14}HgI_2N_6$: C, 32.35; H, 1.73; N, 10.29. Found: C, 32.04; H, 1.51; N, 10.53. ^{1}H NMR: (400 MHz, $(CD_3)_2SO$), δ (ppm): 14.088 (s, 1H), 9.153 (s, 2H), 9.118 (d, $J = 4.4$ Hz, 2H), 8.449 (s, 1H), 8.405 (d, $J = 8.4$ Hz, 2H), 8.182 (s, 2H), 7.985 (d, $J = 8.4$ Hz, 1H), 7.920 (s, 1H), 7.195 (s, 1H).

3. Results and discussion

3.1. *Crystal structure of L*

Single-crystal X-ray diffraction measurements reveal that **L** ($C_{22}H_{14}N_6 \cdot CH_3CH_2OH \cdot H_2O$) and $HgLI_2$ [$Hg(C_{22}H_{14}N_6)I_2$] conform to the space group C2/c

Table 1. Crystallographic data for **L** and $HgLI_2$.

Compound	**L**	$HgLI_2$
Empirical formula	$C_{48}H_{44}N_{12}O_3$	$C_{22}H_{14}HgI_2N_6$
Formula weight	836.36	816.78
Crystal system	Monoclinic	Tetragonal
Space group	C2/c	I4(1)/a
Unit cell dimensions (Å, °)		
a	24.596(5)	28.279(5)
b	13.531(5)	28.279(5)
c	14.285(5)	13.589(5)
β	124.776(5)	90.000(5)
Volume (Å^3), *Z*	3905(2), 4	10867(5), 16
Temperature (K)	298(2)	298(2)
Calculated density (g cm^{-3})	1.451	1.997
Absorption coefficient (mm^{-1})	0.097	7.956
θ range for data collection (°)	2.07–25.00	1.66–25.00
Reflections collected	6569	35,311
Independent reflection	3409	4780
No. parameters refined	287	280
R_1	0.0396	0.0446
wR_2	0.1425	0.1284
Goodness-of-fit on F^2	1.298	0.899

and I4(1)/a (table 1). Molecular structures showing the arrangement about **L** and $HgLI_2$ are shown in figures 1 and 2, respectively.

In the crystal structure of **L**, there is one phen, one EtOH, and one H_2O in each independent crystallographic unit. The dihedral angle between the benzene ring and the imidazole ring at the terminal is 48.67° and 10.56° between the benzene ring and the phen ring. As shown in figure 3(a), **L** generates a 1-D chain along the *b*-axis through N–H···N interactions between two neighboring dimers, where the distance of N4–H4···N7 is 2.093 Å and the angle of N4–H4–N7 is 165.35°. Figure 3(b) shows that water plays a very important role, linking two neighboring dimers generating a 2-D layer along the *c*-axis with a N3–O2–N3 angle of 73.06°. Water molecule also connects to two ethanols through O1–H52···O2 hydrogen bonds (ethanol provided H, d(O1–H52···O2) = 2.110 Å and ∠(O1–O2–O1) = 72.39°). Finally, **L** forms a stable 3-D supermolecular structure through π–π stacking interactions (the shortest distance is 3.258 Å) between neighboring dimers along the *a*-axis (figure 4).

3.2. *Crystal structure of $HgLI_2$*

The asymmetric unit of $HgLI_2$ contains one Hg(II), one phen, and two iodides, as shown in figure 2(a). Each Hg(II) in $HgLI_2$ is primarily coordinated by two nitrogen atoms from phen (Hg–N5 2.379(7) Å; Hg–N6 2.398(7) Å) and two iodides (Hg–I2 2.681(1) Å; Hg–I1 2.694(1) Å) to furnish a distorted tetrahedral coordination geometry, consistent with the literature [28]. Each bond angle around mercury is 70.0(2)–125.8(2)°. Selected bond lengths and angles are listed in table 2. As shown in figure 5, iodide does not participate in forming the framework, different from most coordination frameworks of mercury [29]. However, different from **L**, the dihedral angle between the benzene and the phen rings is 14.53° (larger than the same angle in **L**), and 27.80°

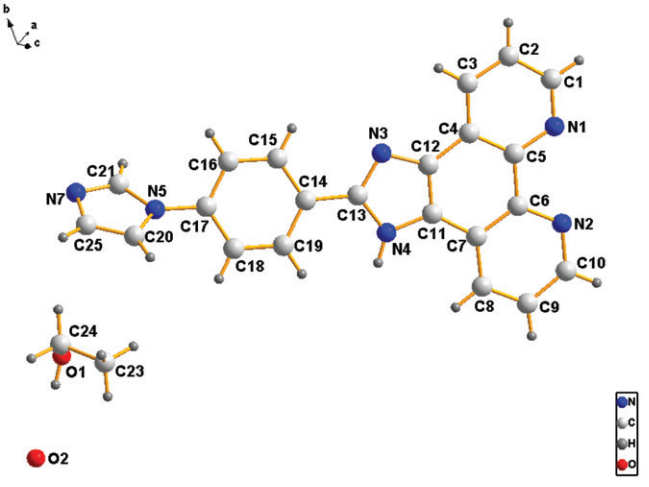

Figure 1. Molecular structure of **L** with an atom-labeling scheme.

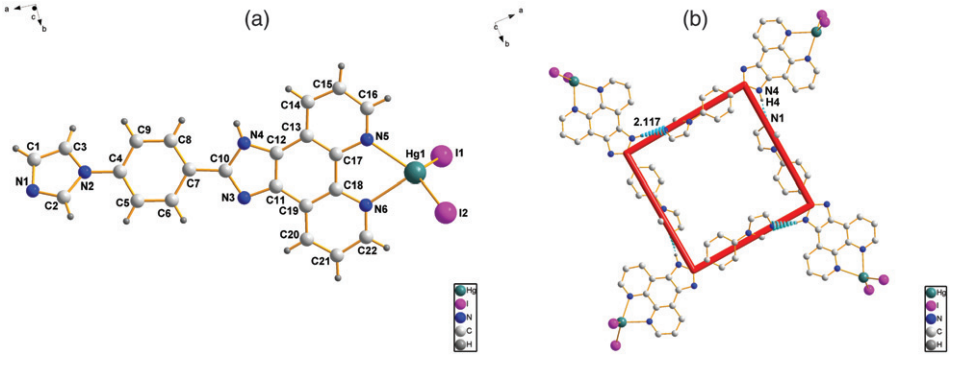

Figure 2. (a) Molecular structure of $HgLI_2$ with atom-labeling scheme. (b) The closed structure of $HgLI_2$ showing the N–H···N hydrogen bond.

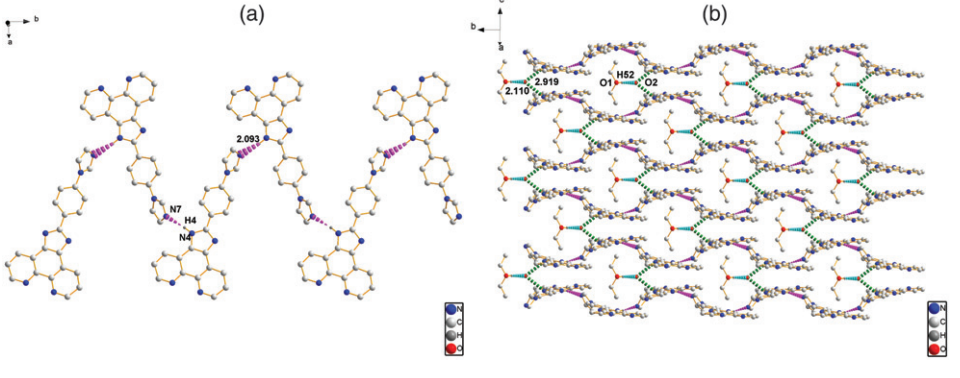

Figure 3. (a) The 1-D chain of **L** showing the N–H···N hydrogen bond along the *b*-axis. Hydrogen atoms except H4 are omitted for clarity. (b) The 2-D layer of **L** showing the O1–H···O2 and O2–H···N hydrogen bond along the *c*-axis. Hydrogen atoms except H4 and H52 are omitted for clarity.

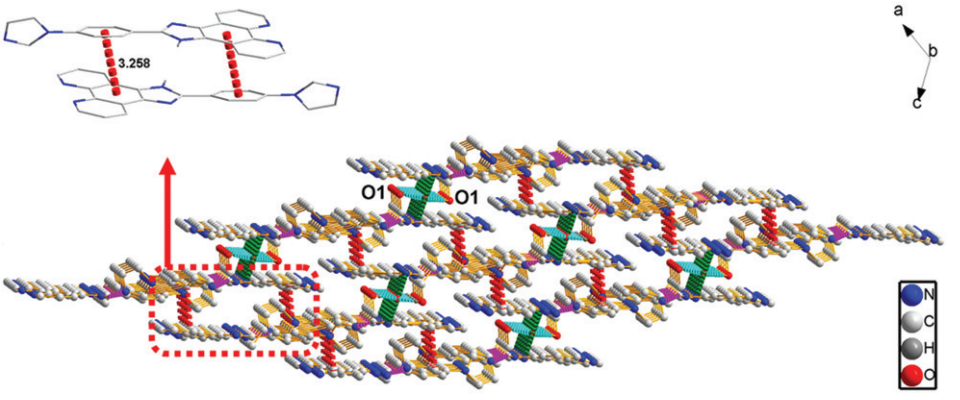

Figure 4. The 3-D supermolecular structure of **L** showing π–π stacking along the *a*-axis. Hydrogen atoms except H4 and H52 are omitted for clarity.

Table 2. Selected bond lengths (Å) and angles (°) for $HgLI_2$.

Hg1–N5	2.379(7)	N5–Hg1–N6	70.0(2)
Hg1–N6	2.398(7)	N5–Hg1–I2	125.8(2)
Hg1–I2	2.681(1)	N6–Hg1–I2	99.9(2)
Hg1–I1	2.694(1)	N5–Hg1–I1	110.1(2)
		N6–Hg1–I1	107.5(2)
		I2–Hg1–I1	123.4(3)

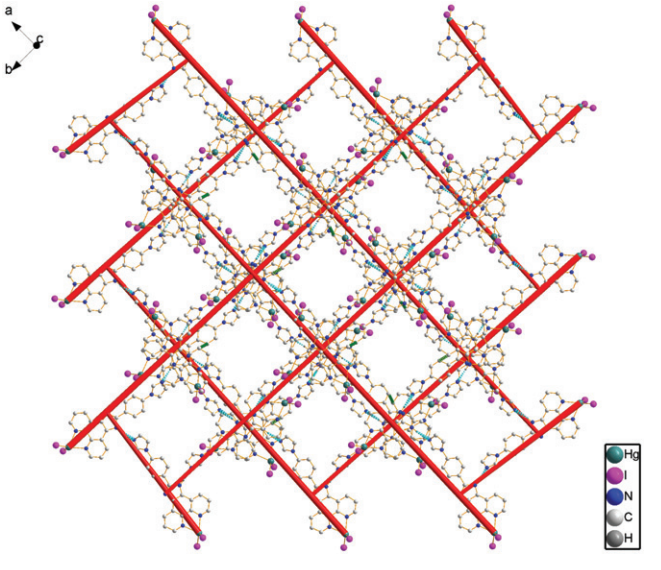

Figure 5. The 3-D supermolecular structure of $HgLI_2$ formed by π–π stacking interactions. Hydrogen atoms except H4 are omitted for clarity.

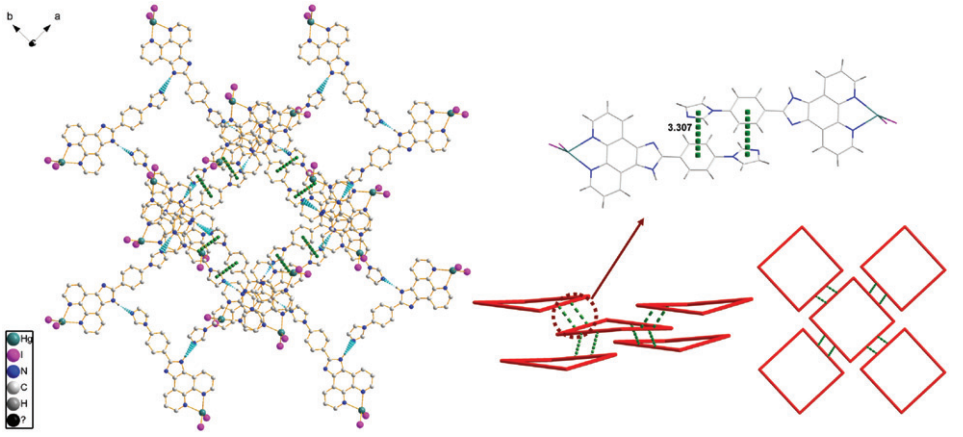

Figure 6. The 2-D layer of $HgLI_2$ formed by π–π stacking interactions. Hydrogen atoms except H4 are omitted for clarity.

(smaller than the same angle in **L**) for the angle between the benzene and the imidazole rings at the terminal. The shortest distance of the π–π stacking contacts (figure 6) between the benzene and the imidazole rings (3.307 Å) at the terminal in $HgLI_2$ is slightly longer than the shortest distance of the π–π stacking contacts in **L** (3.258 Å), perhaps due to iodides. Different from **L**, $HgLI_2$ forms a closed structure through N–H···N bond interactions between two neighboring dimers with a N4–H4···N1 distance of 2.117 Å and a angle of N4–H4–N7 162.40° (figure 2b). The distance of N4–H4···N1 is longer than **L**, while the angle is smaller than **L**. Adjacent closed structures of $HgLI_2$ are further connected by different π–π stacking interactions (the shortest distance is 3.307 Å), generating 2-D and 3-D supermolecular structures (figures 5 and 6).

3.3. *^{1}H NMR Spectra studies*

L and $HgLI_2$ give well-defined ^{1}H NMR spectra, permitting unambiguous identification and assessment of purity. The proton on the nitrogen of imidazole resonates at *ca* δ 13.80 for **L** as a weak broad singlet, characteristic of an active proton, but is observed as a strong narrow singlet at *ca* δ 14.088 for Hg(II) complex. In the ^{1}H NMR spectrum of **L**, signals at δ 13.80, 9.15, 9.11, 8.45, 8.40, 8.18, 7.98, 7.92, and 7.19 can easily be assigned to H(NH), H_a, H_c, H_f, H_d, H_e, H_g, H_b, and H_h, respectively. These chemical shifts of protons of **L** allow the assignment of resonances in $HgLI_2$, as shown in figure 7. Signals of H_a, H_f, H_e, H_g, and H_h experience slight shifts compared to those of free **L**. H_b and H_c show surprisingly large (0.33 and 0.22 ppm) downfield shifts compared to H_c (0.10 ppm). It is probable that the terminal coordinated iodide affects the signal of H_a because of its large radius. The shift in the resonance positions of other protons may be due to the reduced electron density of **L** after coordination with Hg(II) [26, 30, 31].

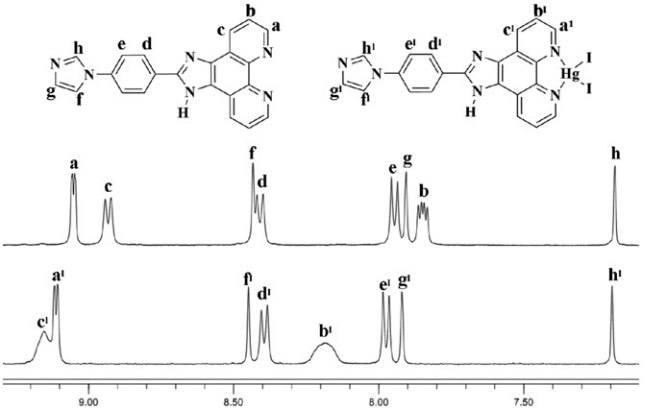

Figure 7. ^{1}H NMR spectra of **L** and $HgLI_2$ in the aromatic region between δ 7.1 and 9.3 [$(CD_3)_2SO$ solvent, TMS reference].

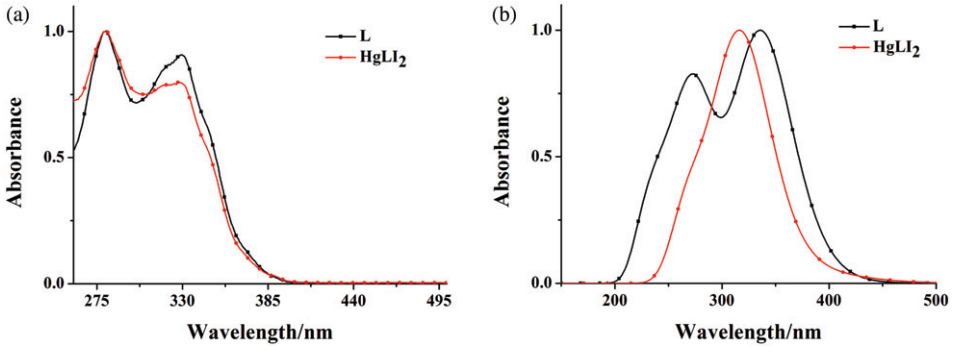

Figure 8. (a) Experimental UV-Vis absorption spectrum. (b) Calculated UV-Vis absorption spectrum.

3.4. *UV-Vis spectra and TD-DFT studies*

The experimental and calculated UV-Vis absorption spectra of **L** and $HgLI_2$ in DMSO are shown in figure 8. Their absorption spectra exhibit two peaks between 280 and 330 nm. **L** and $HgLI_2$ exhibit an absorption at 280 nm from π to π^* transitions; the absorption at 330 nm corresponds to the ICT transition of the main chain [32].

To investigate the geometrical, electronic, and optical properties of **L** and $HgLI_2$ at a molecular level, quantum chemical calculations based on the DFT were performed. The experimental wavelengths (λ_{exp}), calculated wavelengths (λ_{cal}), and dipole moment ($\Delta\mu_{total}$) are given in table 3. Electron distribution of the HOMO and LUMO energy levels of **L** and $HgLI_2$ is shown in figure 9. In the HOMO of **L** and $HgLI_2$, the electrons are mainly spread over the molecule along the molecular axis, while in the LUMO the electrons are mainly concentrated on phenanthroline. In the LUMO of $HgLI_2$, compared with **L**, the delocalizable electrons of phenanthroline were increased. Upon excitation, electrons were mainly transferred from the terminal imidazoles to

Table 3. Experimental wavelengths (λ_{exp}), calculated wavelengths (λ_{cal}), and dipole moment ($\Delta\mu_{total}$) for **L** and $HgLI_2$.

	λ_{exp} (nm)	λ_{cal} (nm)	$\Delta\mu_{total}$ (D)
L	329	335	6.2
	281	272	
$HgLI_2$	327	316	16.3
	280	268	

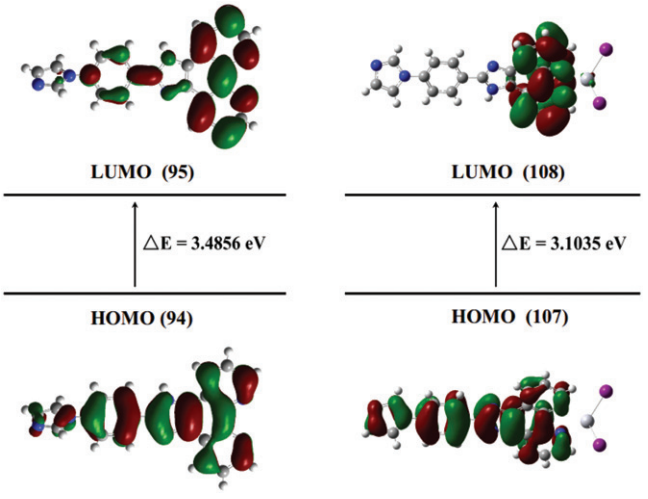

Figure 9. Energy level and electron density distribution of frontier molecular orbitals of **L** and $HgLI_2$.

phenanthroline, showing a strong migration of ICT character. The calculations also show that $HgLI_2$ has large molecular dipole moment ($\Delta\mu_{total} = 16.3$ D). Obviously, it has a strong interaction in the solid state, which results in fluorescence quenching of $HgLI_2$. As shown in table 3 and figure 8, the calculated absorption spectra display a qualitative agreement in the relative locations of the absorptions with the experimental observations.

3.5. *Solid-state luminescence emission*

Solid-state luminescence of **L** and $HgLI_2$ were investigated at room temperature (figure 10). $HgLI_2$ emits a weak blue color with a maximum at 522 nm upon excitation at 320 nm. Comparing with **L**, the emission of $HgLI_2$ is 52 nm red-shifted. This may be caused by a change in the HOMO and LUMO energy levels of neutral ligands coordinating to metal centers. Proved by X-ray structures, the ligand molecules became more planar after coordination with Hg^{2+}. The main emission band of **L** is attributed to fluorescence emission stemming from the ligand-centered π–π^* transition, while the main emission band of $HgLI_2$ may be tentatively attributed to metal-to-ligand charge transfer (MLCT) and π–π^* transition of phenanthroline.

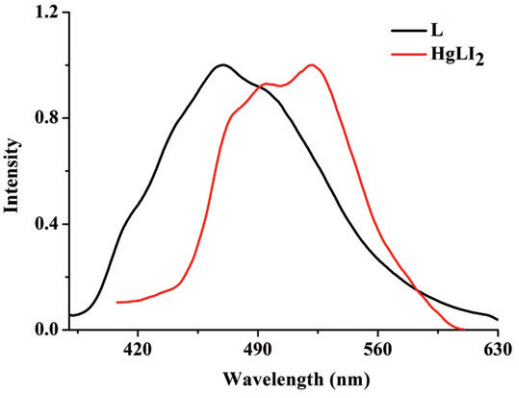

Figure 10. Solid-state luminescence spectra of **L** and $HgLI_2$.

4. Conclusions

A new complex has been prepared from an asymmetric **L** and Hg(II). Single-crystal X-ray diffraction measurement shows the structure of **L** and $HgLI_2$. Solvent and various weak interactions, including hydrogen bonds (N–H···N, O–H···O and O–H···N) and π–π contacts play significant roles in the final supermolecular structures. ^{1}H NMR spectra of **L** and $HgLI_2$ were assigned. The experimental study gives reasonable interpretation for photophysical properties based on crystallographic data, which is supported by DFT calculations.

Supplementary material

Full crystallographic data in CIF format for **L** and $HgLI_2$ have been deposited with the Cambridge Crystallographic Data Centre (CCDC No. 848573 and CCDC No. 870552). Copies of the data can be obtained, free of charge, on application to CCDC, 12 Union Road, Cambridge, CB2 1EZ, U.K; Fax: +44(0)-1223-336033; or E-mail: deposit@ccdc.cam.ac.uk

Acknowledgments

This work was supported by Program for New Century Excellent Talents in University (China), Doctoral Program Foundation of Ministry of Education of China (20113401110004), National Natural Science Foundation of China (21071001, 21102001, 21101001, 21271003), Education Committee of Anhui Province (KJ2012A024), the Team for Scientific Innovation Foundation of Anhui Province (2006KJ007TD), the 211 Project of Anhui University, Ministry of Education Funded Projects Focus on Returned Overseas Scholar.

References

[1] Y.-W. Li, J.-P. Zhao, L.-F. Wang, X.-H. Bu. *CrystEngComm*, **13**, 6002 (2011).
[2] X.-F. Wang, Y.-B. Zhang, X.-N. Cheng, X.-M. Chen. *CrystEngComm*, **10**, 753 (2008).
[3] D. Han, F.-L. Jiang, M.-Y. Wu, L. Chen, Q.-H. Chen, M.-C. Hong. *Chem. Commun.*, **47**, 9861 (2011).
[4] X. Tan, J.-X. Zhan, J.-Y. Zhang, L. Jiang, M. Pan, C.-Y. Su. *CrystEngComm*, **14**, 63 (2012).
[5] W.-G. Lu, C.-Y. Su, T.-B. Lu, L. Jiang, J.-M. Chen. *J. Am. Chem. Soc.*, **128**, 34 (2006).
[6] S.-S. Chen, M. Chen, S. Takamizawa, M.-S. Chen, Z. Su, W.-Y. Sun. *Chem. Commun.*, **47**, 752 (2011).
[7] L.-L. Liang, S.-B. Ren, J. Zhang, Y.-Z. Li, H.-B. Du, X.-Z. You. *Cryst. Growth Des.*, **10**, 1307 (2010).
[8] F.-Y. Meng, Y.-L. Zhou, H.-H. Zou, M.-H. Zeng, H. Liang. *J. Mol. Struct.*, **920**, 238 (2009).
[9] D. Braga, L. Brammer, N.-R. Champness. *CrystEngComm*, **7**, 1 (2005).
[10] C.-J. Kepert. *Chem. Commun.*, 695 (2006).
[11] X.-X. Xu, Y. Lu, E.-B. Wang, Y. Ma, X.-L. Bai. *Inorg. Chim. Acta*, **360**, 455 (2007).
[12] J. Yang, J.-F. Ma, S.-R. Batten, Z.-M. Su. *Chem. Commun.*, 2233 (2008).
[13] Z.-X. Li, Y. Xu, Y. Zuo, L. Li, Q. Pan, T.-L. Hu, X.-H. Bu. *Cryst. Growth Des.*, **9**, 3904 (2009).
[14] Y. Liu, V.-C. Kravtsov, M. Eddaoudi. *Angew. Chem. Int. Ed.*, **47**, 8446 (2008).
[15] C.-N.-R. Rao, S. Natarajan, R. Vaidhyanathan. *Angew. Chem. Int. Ed.*, **43**, 1466 (2004).
[16] S. Kitagawa, R. Kitaura, S.-I. Noro. *Angew. Chem. Int. Ed.*, **43**, 2334 (2004).
[17] P.-J. Hagrman, D. Hagrman, J. Zubieta. *Angew. Chem. Int. Ed.*, **38**, 2638 (1999).
[18] A.-J. Blake, N.-R. Champnees, P. Hubberstey, W.-S. Li, M.-A. Withersby, M. Schröder. *Coord. Chem. Rev.*, **183**, 117 (1999).
[19] B. Moulton, M.-J. Zaworotko. *Chem. Rev.*, **101**, 1629 (2001).
[20] S.-L. Zheng, J.-P. Zhang, X.-M. Chen, Z.-L. Huang, Z.-Y. Lin, W.-T. Wong. *Chem. Eur. J.*, **9**, 3888 (2003).
[21] E. Freire, S. Baggio, R. Baggio, L. Suescun. *J. Chem. Crystallogr.*, **29**, 825 (1999).
[22] C.-W. Chan, S.-M. Peng, C.-M. Che. *Inorg. Chem.*, **3**, 3656 (1994).
[23] G.-M. Cockrell, G. Zhang, D.-G. VanDerveer, R.-P. Thummel, R.-D. Hancock. *J. Am. Chem. Soc.*, **130**, 1420 (2008).
[24] A.-L. Beauchamp, B. Saperas, R. Rivest. *Can. J. Chem.*, **49**, 3579 (1971).
[25] F. Ramezanipour, H. Aghabozorg, J. Soleimannejad. *Acta Cryst.*, **61**, 1194 (2005).
[26] H. Chao, R.-H. Li, C.-W. Jiang, H. Li, L.-N. Ji, X.-Y. Li. *J. Chem. Soc., Dalton Trans.*, 1920 (2001).
[27] L. Yang, J.-K. Feng, A.-M. Ren. *J. Org. Chem.*, **70**, 5987 (2005).
[28] H.-P. Zhou, P. Wang, L.-X. Zheng, W.-Q. Geng, J.-H. Yin, X.-P. Gan, G.-Y. Xu, J.-Y. Wu, Y.-P. Tian, Y.-H. Kan, X.-T. Tao, M.-H. Jiang. *J. Phys. Chem. A*, **113**, 2584 (2009).
[29] H.-P. Zhou, F.-X. Zhou, P. Wu, Z. Zheng, Z.-P. Yu, Y.-X. Chen, Y.-L. Tu, L. Kong, J.-Y. Wu, Y.-P. Tian. *Dyes Pigm.*, **91**, 237 (2011).
[30] H. Chao, R.-H. Li, B.-H. Ye, H. Li, X.-L. Feng, J.-W. Cai, J.-Y. Zhou, L.-N. Ji. *J. Chem. Soc., Dalton Trans.*, 3711 (1999).
[31] Y.-H. Gao, J.-Y. Wu, Q. Zhao, L.-X. Zheng, H.-P. Zhou, S.-Y. Zhang, J.-X. Yang, Y.-P. Tian. *New J. Chem.*, **33**, 607 (2009).
[32] H.-G. Zhang, X.-T. Tao, K.-S. Chen, C.-X. Yuan, S.-N. Yan, M.-H. Jiang. *Chin. Chem. Lett.*, **22**, 647 (2011).